Springer

KSME

Journal of Mechanical Science and Technology 30 (9) (2016) 4015~4022
www.springerlink.com/content/1738-494x(Print)/1976-3824(Online)
DOI 10.1007/s12206-016-0814-1

A bidirectional valveless piezoelectric micropump with three chambers applying synthetic jet †

Xiuhua He*, Liang Xu, Xitong Zhang and Song Yang

School of Energy and Power Engineering, Jiangsu University, Zhenjiang, Jiangsu, China

(Manuscript Received November 18, 2015; Revised March 18, 2016; Accepted March 31, 2016)

Abstract

A new type of valveless piezoelectric micropump is presented. Synthetic jet and Coanda effect are utilized to achieve larger and bidirectional flow rate. The numerical simulation applying the velocity and pressure boundary conditions as well as the SST turbulence model were utilized to research the performance and internal flow state of the micropump. The simulation method was tested by the previous experimental data and the results matched well. The results suggest that the flow rate of the micropump is related to the Reynolds number and frequency. The entrainment flow rate of synthetic jet accounts for over 80% of the total outflow rate. The outflow rate is much larger than the volume change of the micropump chambers. There is an optimal frequency to obtain the maximum flow rate regarding the volume change of the chambers as a constant. The fluctuation of the flow rate decreases with the increase of frequency. When the frequency is higher than 25 Hz, the outflow can be continuous. Working at the Reynolds number of 1000 and optimal frequency of 50 Hz, the flow rate is 6.8 ml/min.

Keywords: Coanda effect; Numerical simulation; Synthetic jet; Valveless micropump

1. Introduction

There is a promising future for Micro-fluidic system in the life sciences and chemical analysis fields such as pathological analysis, DNA sequencing and drug interactions [1-3]. Some great technologies like gene chip and biochip are developed by the system and now applied in the aforementioned and other fields [4, 5]. Micropumps function as crucial device supplying the energy for the fluid to overcome the resistance of the system. Micropumps can be classified into mechanical and non-mechanical ones generally according to the principle that how the fluid is transported [6]. Non-mechanical micropumps such as the electroosmotic [7], magnetohydrodynamic [8], and electrowetting [9] micropumps drive the fluid directly by electric, magnetic or other types of energy without moving parts. However, they are not widely utilized for the complex structures and the relatively harsh working conditions as well as the low outlet pressure [10]. The mechanical micropumps work with vibrating diaphragms or rotating parts [11, 12], for instance, the vibrating diaphragm micropumps [13], rotary micropumps [14], and ferrofluid micropumps [15]. The piezoelectric micropumps belonging to the vibrating diaphragm micropumps may utilize valves to control the flow direction. However, there are lots of disadvantages for micropumps with valves such as the performance reduction, unreliability because of wear and fatigue of the valves, high pressure loss near the check valves and a risk of valve clogging [16].

Many researchers have focused on the piezoelectric micropumps with no moving valves over the last few decades for the simple structure and great miniaturization potential. There is also a great advantage for the valveless piezoelectric micropumps to transport the solution containing large cells or particles which are easy to cause valve clogging [17]. The valveless micropump based on diffuser/nozzle element is one of the most-investigated type of valveless piezoelectric micropumps so far. In 1993, the first valveless micropump based on diffuser/nozzle with small diffuser angle was fabricated by Stemme and Stemme [18]. The oscillating chamber volume produced by a vibrating diaphragm and the unique diffuser/nozzle element make the micropump work. There are a lot of researches have been reported on this type of micropumps [18, 19]. The diffuser/nozzle element is the vital structure of the micropumps. However, at low Reynolds numbers, the loss coefficients of nozzle/diffuser will be close which means the flow rate and volumetric efficiency will be low under this circumstance.

The synthetic jet as well as Coanda effect have been researched in the micropump field to improve the flow rate and

*Corresponding author. Tel.: +86 13862446132
E-mail address: xiuhua.he@ujs.edu.cn
This paper was presented at the AJK2015-FED, Seoul, Korea, July 2015.
† Recommended by Guest Editor Gihun Son and Hyoung-Gwon Choi

efficiency. A classic synthetic jet actuator is usually composed of a sealed cavity with a flexible diaphragm on one side and an orifice on the other side. The diaphragm vibrates by driving voltage to change the volume of the cavity. In the suction stage, the diaphragm driven towards the opposite direction of orifice, fluid will be drained into the cavity. The discharge stage is that the diaphragm driven toward the orifice, making the ejection of fluid through the orifice. A series of vortexes appear at the edge of the orifice because of the shear force and keep moving far away from the orifice and would not be effected by the next suction stroke, which means the synthetic jet is a zero-net-mass-flux jet but also a nonzero momentum-flux jet [20]. The Coanda effect which was first discovered by Henri Coanda in early 20th century is applied in the study. Energy exchange happens between jet and the surrounding fluid, then jet entrains fluid. However, the flow of the entrainment is restricted by the wall of the confined space, leading to the pressure difference between the wall and the jet. The deflection of the jet which caused by the pressure difference makes the jet attach to the boundary [21, 22].

Luo et al. presented a valveless micropump applying synthetic jet in 2001 [23]. In 2011, a synthetic jet-type micropump for transporting air was presented by Jong et al. [24], the optimal structure parameters of this micropump were determined by numerical analysis. In 2014, a Coanda effect-type micropump was proposed by Yang et al. [25]. This kind of micropump has a larger volume efficiency than normal ones which could be over 50%. In 2015, a valveless micropump applying synthetic jet which can achieve bidirectional flow rate was designed by Zhang et al. [26], the direction control of the flow could be achieved by controlling the excitation voltages on the two piezoelectric actuators. However, the excitation voltage on one actuator has to be much less than the other one in order to make the difference between two actuators' displacements for generating the Coanda effect, which means the flow rate mainly depends on only one actuator. Therefore, the volumetric efficiency of this micropump is not improved much compared with the micropump with single chamber.

The numercial simulation is used to study a new type of micropump which can transport the liquid bidirectionally in this research. The advantages of larger flow rate and continuous outflow make it more efficient than nozzle/diffuser micropumps under some circumstances [27]. Furthermore, the flow direction can be changed by controlling the excitation voltages of three piezoelectric actuators (strong voltages on two actuators and weak voltage on the rest one). The total displacements of the two actuators is much lager than only one actuator, so the flow rate of the micropump with three chambers is much lager than which with only two. The comparison between the micropumps with two and three chambers has been done, it shows that the flow rates of each micropump are 1.9 ml/min and 6.8 ml/min at the optimal working conditions respectively. And the volumetric efficiency λ of the micropumps with two and three chambers can be 0.99 and 1.8, respectively. Both volume change of chambers and instantaneous flow rates of the micropumps with two and three chambers are shown as Fig. 1 regarding each chamber's volume change as a constant of 1.92 ml/min.

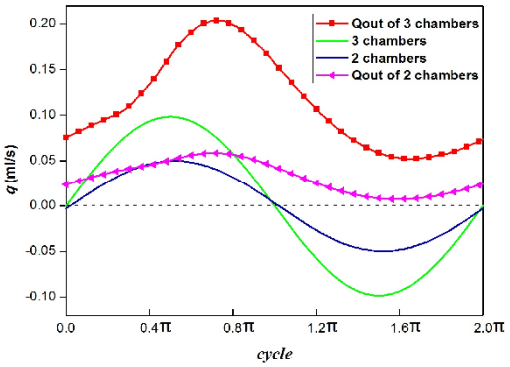

Fig. 1. Volume change of the chambers and outflow rates of micropumps with two and three chambers in a cycle (volume change for each chamber is 1.92 ml/min, f = 50 hz).

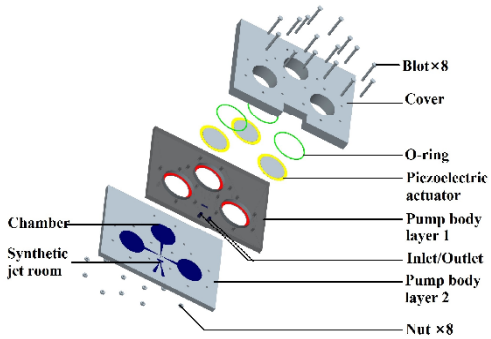

(a)

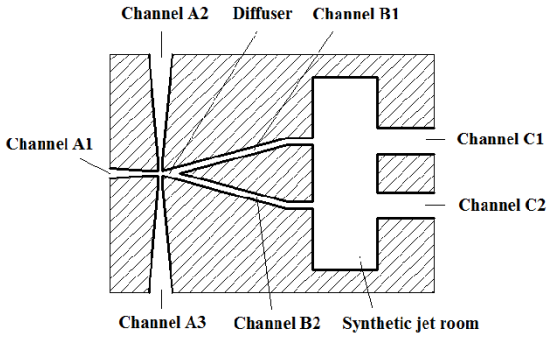

(b)

Fig. 2. (a) Structure of micropump; (b) structure of synthetic jet element.

2. Structure and principle

2.1 Structure

Fig. 2(a) shows the structure of the micropump. It is composed of two pump body layers and a cover. The pizeoelectric actuators are set in the cover. The inlet and outlet are fabricated in the body layer 1 while the synthetic jet element as well as three chambers are manufactured in the layer 2. The

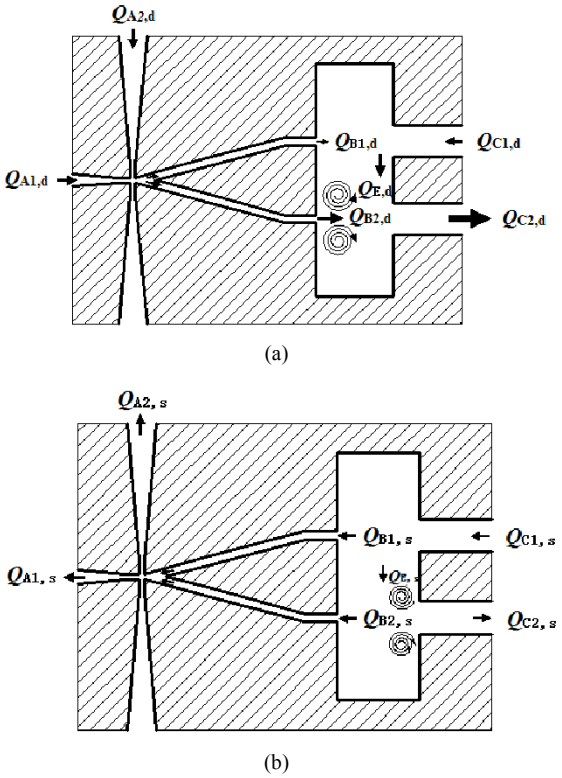

Fig. 3. (a) Discharge stage; (b) suction stage.

silicon, glass or PMMA can be used to fabricate the pump body as well as cover which will be bonded together by anodic bonding or adhesive.

Fig. 2(b) shows the structure of synthetic jet element which is crucial to the micropump. Pump chamber 1, chamber 2 and chamber 3 and the diffuser are connected by the channel A1, A2 and A3, respectively. The diffuser and the synthetic jet room are connected by channel B1and B2. The channel C1 and C2 are set after the synthetic jet room, connecting with the inlet and the outlet, respectively.

2.2 Principle

For example, the actuator 1 and the actuator 2 are excited by the same synchronous voltages while the actuator 3 stays static. According to the Coanda effect, pressure difference occurs in the diffuser which makes jet flow attach to channel B2. Therefore the actuator 1 functions as the power element and the actuator 2 serves as the power element as well as the controller of the pump direction. As the actuators oscillating, they alternatively draw in or blow out the ambient fluid. According to the pattern of the actuators, a working cycle can be divided into two stages, the discharge stage and the suction stage as shown in Fig. 3.

Fig. 3(a) shows the diagram of discharge stage. The $Q_{A2,d}$ is equal to $Q_{A1,d}$ due to the same driving voltage. The maximum volume change V of the pump chamber connected with the channel A1 and channel A2 is set as

$$V = Q_{A2,d} = Q_{A1,d} . \quad (1)$$

Impacted by the discharging of the fluid which from the vertical direction, the fluid from the channel A1 turns to the channel B2, producing a pressure differential in the diffuser area. The jet flow is forced to attach the wall of the diffuser speedily because of the Coanda effect. Therefore, $Q_{B2,d}$ is larger than $Q_{B1,d}$ significantly because most of fluid is draining into the channel B2 during this stage. So, the relationship between $Q_{B2,d}$ and $Q_{B1,d}$ is

$$Q_{B1,d} = \beta Q_{B2,d} (0 < \beta << 1) . \quad (2)$$

Based on continuity equation

$$Q_{A1,d} + Q_{A2,d} = Q_{B1,d} + Q_{B2,d} . \quad (3)$$

Based on Eqs. (1)-(3), it is found that

$$Q_{B2,d} = \frac{2V}{1+\beta} . \quad (4)$$

In the synthetic jet room, the main jet flow from the channel B2 produces a series of vortexes entraining the fluid drained out of the channel B1 and sucking from the channel C1 as well. The main jet flow from the channel B2 as well as the entrainment fluid are supposed to enter into the channel C2 and then flow out through the outlet. The total outflow rate can be expressed as

$$Q_{C2,d} = Q_{E,d} + Q_{B2,d} . \quad (5)$$

Using Eqs. (4) and (5), $Q_{C2,d}$ will be got as

$$Q_{C2,d} = Q_{E,d} + \frac{2V}{1+\beta} . \quad (6)$$

The suction stage is shown in Fig. 3(b). Because of the symmetry of the structure, the flow rates drains into the channel B1 and B2 are nearly the same. We set

$$Q_{B1,s} = Q_{B2,s} = V . \quad (7)$$

Simultaneously, the vortexes generated within discharge stage still exist during this stage and continue entraining the fluid from channel C1 to channel C2. Thus $Q_{C2,s}$ can be calculated as

$$Q_{C2,s} = 2V - Q_{C1,s} = -Q_{E,s} . \quad (8)$$

The outlet flow rate Q_{out} can be obtained by Eq. (9) using Eqs. (6) and (8)

$$Q_{out} = Q_{C2,d} - Q_{C2,s} = \frac{2}{1+\beta} V + Q_{E,d} + Q_{E,s} . \quad (9)$$

Define λ as the volumetric efficiency, which means the ratio of the outlet flow rate to the volume change of the pump chambers in a cycle.

$$\lambda = \frac{Q_{out}}{2V} = \frac{1}{1+\beta} + \frac{Q_E}{2V} \tag{10}$$

where

$$Q_E = Q_{E,d} + Q_{E,s} \,. \tag{11}$$

The first term $\frac{1}{1+\beta}$ in the Eq. (10) describes the volumetric efficiency attributed to the Coanda effect for the only relative coefficient β. The second term $\frac{Q_E}{2V}$ describes the contribution of the synthetic jet. It suggests that the outflow performance of the micropump is attributed to both of the Coanda effect and synthetic jet.

What is more, when the actuator 2 stays static and the actuator 3 vibrates as the power and the controlling element of the pump flow instead, the flow direction changes. In the meantime, the characteristic of the micropump will not change because the synthetic jet element is symmetrical. Therefore, the bidirectional pump flow can be achieved through choosing the actuator 2 or actuator 3 to vibrate alternatively.

3. Numerical simulation

3.1 Flow model and boundary condition setting

In order to obtain the internal flow state as well as the flow rate within the micropump, a numerical simulation was done with the medium of incompressible water at ordinary temperature. Define the Reynolds number as:

$$Re = \frac{\left(\frac{4A}{\chi}\right)u}{\upsilon} = \frac{du}{\upsilon} \tag{12}$$

where χ and A are the wetted perimeter and area of the diffuser throat, respectively; u is the mean velocity on the section plane of the throat; υ is the kinematic viscosity of the media. Table 1 shows the structural size of the synthetic jet element. In this simulation, as the Reynolds number ranged from 250 to 1000, the flow model used the SST turbulence model for calculating the flow in the boundary layer more properly [28-30].

Fig. 4. illustrates the simulation domain and the boundary locations. The 'Chamber 1' and 'Chamber 2' were set as 'velocity Inlet' , whose values were calculated by the Eq. (13) to model the vibration of the piezoelectric diaphragms stimulated by the the sinusoidal alternating voltage. The 'Inlet 'and 'Outlet' were set as the 'Pressure outlet', whose pressure were set as 1 atm. The overall grid number reached as much as about 2000000.

Table 1. Structural size of synthetic jet element.

Structural symbol	Value
θ(°)	90
L_A (μm)	1100
d_d (μm)	100
L_d (μm)	400
θ_d(°)	30
h_B (μm)	150
d_{AB} (μm)	100
y_B (μm)	1500
h_C (μm)	600
d_C (μm)	600
l_s (μm)	1500
d_s (μm)	4500
h_s (μm)	1000
D (μm)	1000

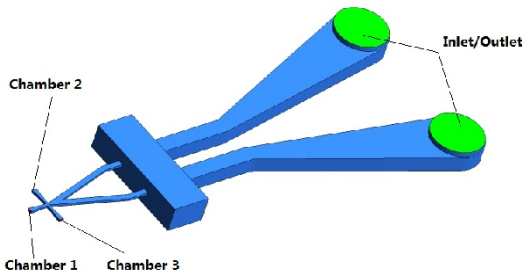

Fig. 4. Simulation domain.

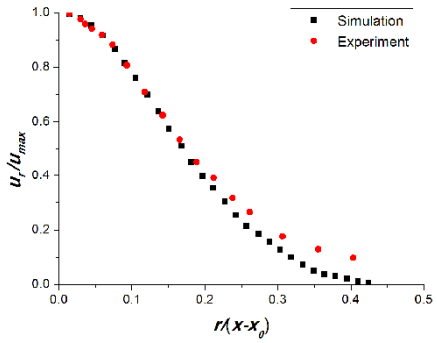

Fig. 5. Comparison of the simulation with experimental normalized velocity profiles.

$$U = U_m \sin\left(\frac{2\pi}{T}t\right) = U_m \sin\left(2\pi ft\right) \tag{13}$$

where U_m means the maximum mean velocity in the section plane of the boundary condition; T is the time of a cycle and its reciprocal f is the stimulating frequency.

The boundary conditions and the flow model were tested by the comparison with the previous experiment data applied by Krishnan and Mohseni [20]. The relevant parameters in the testing simulation are referred to the paper reported by them. The working media was incompressible air at normal tem-

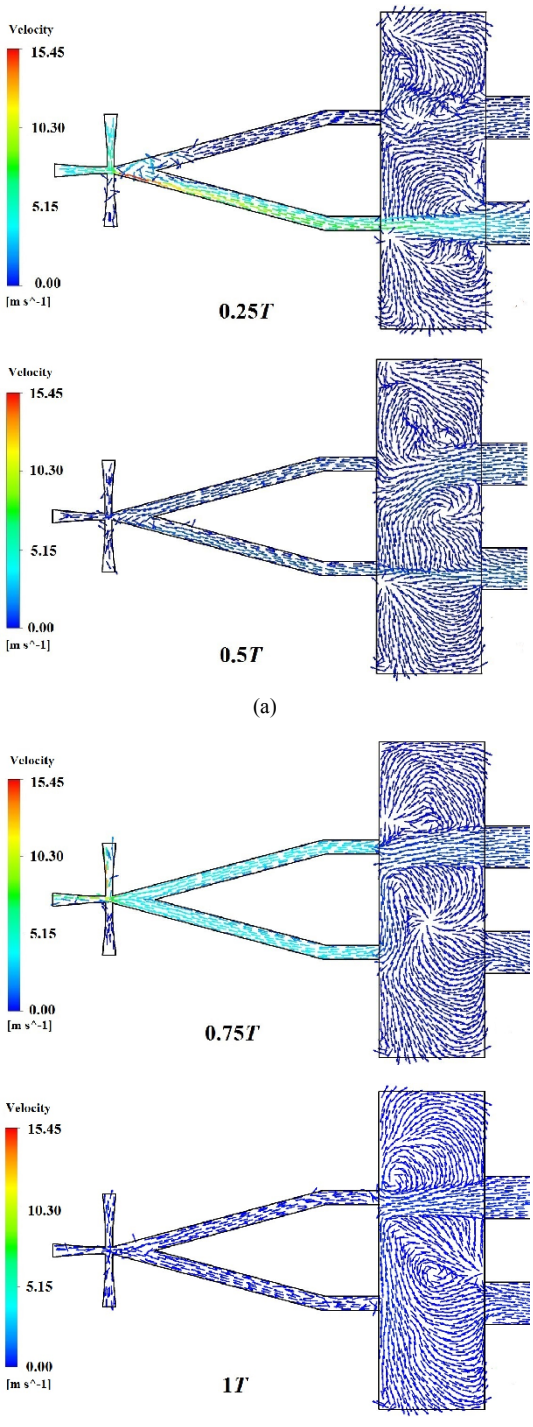

Fig. 6. (a) Flow state of discharge stage in the diffuser and the synthetic jet room in a cycle; (b) flow state of suction stage in the diffuser and the synthetic jet room during a cycle (Re = 1000, f = 50 hz).

perature. Fig. 5 illustrates the comparison of the normalized streamwise velocity profiles u_r/u_{max} at the distance of 15 d_d from the virtual origin x_0 in cylindrical coordinates between the simulation and the experimental results respectively, where d_d is the diameter of the synthetic jet actuator exit; u_r is the velocity along radical direction; u_{max} is the maximum of u_r, x_0 is the virtual origin based on velocity.

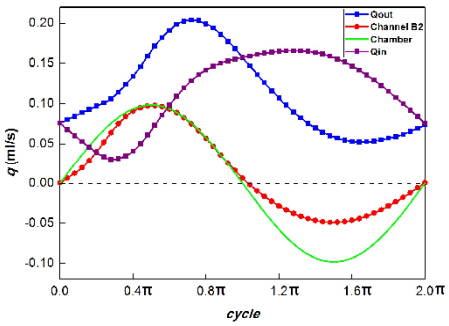

Fig. 7. Volume change of the chamber, flow rates of channel B2 and outlet during a cycle (Re = 1000, f = 50 hz).

3.2 Results and discussion

Fig. 6 shows the internal flow state in the diffuser and the synthetic jet room at four specific moments of a cycle when Re = 1000 and f = 50 Hz. The first half of the period is discharge stage and the second half is suction stage. The Coanda effect appears at 0.25 T in the diffuser. Simultaneously, a series of vortexes generated by the main jet from channel B2 move downstream with the jet, and retrain the fluid through channel C1 and the channel B1. There is a speed reduction of the fluid in the channel B2 during 0.25T to 0.5T. However, the vortexes are still strong enough to suck more fluid from channel C1. From 0.5T to 1T, the fluid sucked from the channel B1 and B2 into the diffuser is equal. In the synthetic jet room, the vortexes continue dissipating but still entraining fluid from the channel C1 during 0.75 T to 1 T.

Fig. 7 illustrates the volume change of the pump chambers and instantaneous flow rates of the channel B2 as well as the outlet in a cycle when Re is 1000 and frequency is 50 Hz. q > 0 indicates the fluid is drained out of channel B2 or outlet. On the contrary, q < 0 means that fluid is drained into the channel.

The results demonstrate the continuous pump flow during a whole cycle can be achieved for the instantaneous flow rate of the outlet is all positive. It is obvious that the flow rate curve of outlet is always above channel B2. That indicates the jet entrains fluid in the synthetic jet room all the time. The flow rate of channel B2 is 0.82 ml/min, and the outlet is 6.8 ml/min. The jet entrainment Q_E contributes most to the final outlet flow rate in this situation for about 88%. The λ is calculated to be 1.8 which means the outlet flow rate is 1.8 times to the volume change of the pump chambers.

The Reynolds number is found to be a essential dimensionless number which affects the function of the micropump strongly. Fig. 8 shows the flow rates of outlet and channel B2 as well as λ at different Res. With the increase of Reynolds number, the flow rates of the channel B2 increases very slowly, but there is approximate linear correlation of the outlet flow rates as the Re increases from 250 to 1000. It reveals the great improvement of the outlet flow rate chiefly because of

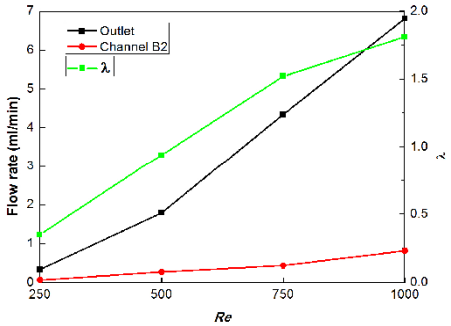

Fig. 8. Flow rates of outlet and channel B2 and λ at different *Re*s.

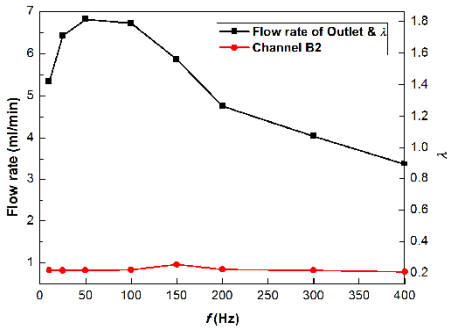

Fig. 9. Flow rates of outlet and channel B2 and λ at different frequencies (*Re* = 1000).

the large growth of the entrainment flow rate which caused by the synthetic jet. For the same reason, the λ can be over 1 when the *Re* is larger than 500, and comes to 1.8 as *Re* = 1000.

Fig. 9 illustrates the flow rates of the outlet and the channel B2 as well as the λ of the micropump at different driving frequencies (10 Hz-400 Hz) when *Re* = 1000. Based on the method of the numerical simulation utilized here, the volume change of the pump chambers (1.88 ml/min when the Re = 1000) per unit time is a constant if the *Re* is invariable. Therefore, the curves of the outlet flow rate and the λ share the same shape as shown in the figure. The flow rate of the outlet can reach the maximum value as f = 50 Hz, and then decreases if the frequency is higher or lower than 50 Hz. However, as the frequency increases, the flow rate through the channel B2 remains very low and almost unchanged. The results suggest that there is an optimal driving frequency to obtain the maximum flow rate for this type of micropump (it is 50 Hz in this case). Moreover, the frequency impacts little on the flow rate caused by Coanda effect, but a lot on the entrainment flow rate, which contributes most to the flow rate of the outlet.

Fig. 10 shows the instantaneous flow rates of the outlet at various frequencies (10 - 400 Hz) as Re = 1000. It reveals that the fluctuation of the flow rate decreases while the frequency increases. Generally, the outflow rate with f = 400 Hz (0.0075 ml/s < q_{out} < 0.10 ml/s) is much lower than that with f = 10 Hz (-0.033 ml/s < q_{out} < 0.31 ml/s). The curve of the flow rate with f = 400 Hz (0.0075 ml/s < q_{out} < 0.10 ml/s) is more smooth than that with f = 10 Hz (-0.033 ml/s < q_{out} < 0.31 ml/s). And it is found out that the curve is always above zero line when f > 25 Hz which means the continuous outflow can be realized under this circumstance.

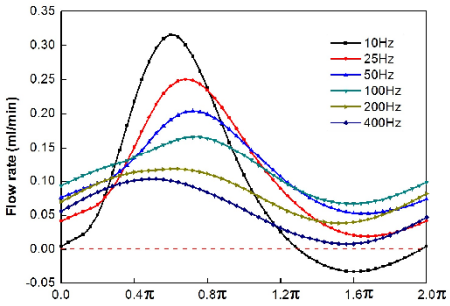

Fig. 10. Instantaneous flow rates of outlet at different frequencies (*Re* = 1000).

4. Conclusions

A new type of micropump which can transport liquid bidirectionally has been designed. It has the advantage of large flow rate as much as 6.8 ml/min when *Re* = 1000 and f = 50 Hz. Furthermore, the flow direction can be controlled using Coanda effect which functions by choosing two piezoelectric actuators of three to be the active ones.

The results obtained by numerical simulation show the entrainment flow rate Q_E always exists during the whole cycle and plays a crucial role in the final outlet flow rate. Since the volume change of the chambers is much lower than the outlet flow rate, so λ can be over 1.

The micropump can achieve higher flow rate and λ as the *Re* increases. The outlet flow rate nearly increases linearly with the increasing *Re*, mainly because of the great improvement of the entrainment flow rate caused by the synthetic jet.

The maximum flow rate and λ for this type of micropump can be obtained at an optimal frequency when the volume change of the chambers is a constant. The frequency impacts little on the flow rate caused by Coanda effect, but a lot on the entrainment flow rate. Moreover, the fluctuation of flow rate decreases with the increase of frequency. When f > 25 Hz, the micropump can achieve continuous outflow.

This kind of micropump can be applied in the Micro-fluidic system especially for chemical analysis, sample injection, mixing and segregation et al. The large, continuous outflow of this valveless piezoelectric micropump meets the requirements of transporting fluid in the Micro-fluidic system and improves its efficacy as well. The micropump is able to realize the bidirectional transport in the system.

Acknowledgment

This work was supported by the project of the National Natural Science Foundation of China [Grant number: 51276082], Departments of Education and Finance, Jiangsu Province of P.R.China (A Project Funded by the Priority Aca-

demic Program Development of Jiangsu Higher Education institutions, PAPD) [grant number: SUZHENGBANFA (2014) No.37].

Nomenclature

A : Area of diffuser throat
D : Inlet and outlet diameter
D_a : Outlet diameter of synthetic jet actuator
d_{AB} : Depth of channel A1, A2, B1, B2; diffuser
d : Diameter of the synthetic jet actuator exit
d_C : Width of channel C1 and C2
d_d : Width of diffuser throat
ds : Width of synthetic jet room
f : Frequency
h_B : Width of channel B1 and channel B2
h_C : Depth of channel C1 and C2
hs : Depth of synthetic jet room
L_A : Length of channel A1 and A2
L_d : Length of diffuser
ls : Length of synthetic jet room
Q : Local flow rate
Q_{out} : Outlet flow rate during a cycle
Q_E : Entrained flowrate caused by synthetic jet in a cycle
q_{out} : Instantaneous outlet flowrate
r : Length in radius direction
T : Time of a cycle
U : Mean velocity applied in boundary condition
U_m : Max mean velocity applied in boundary condition
u : Mean velocity in throat cross section
u_a : Axial velocity on the axial of synthetic jet actuator
u_r : Mean velocity along radical direction
V : Volume change of pump chambers
y_B : Distance from channel B1 to channel B2
β : Ratio of the $Q_{B2,d}$ to $Q_{B1,d}$
θ : Angle of channel A1 and A2
θ_d : Diffuser angle
λ : Volumetric efficiency
υ : Kinematic viscosity of water
χ : Wetted perimeter of the diffuser throat
x_0 : Virtual origin based on velocity

References

[1] E. Verpoorte, Microfluidic chips for clinical and forensic analysis, *Electrophoresis*, 23 (2002) 677-712.
[2] P. Dario, N. Core, M. C. Carrozza and G. Varallo, A fluid handling system for a chemical microanalyzer, *Journal of Micromechanics and Microengineering*, 6 (1996) 95-98.
[3] E. M. J. Verpoorte, B. H. Van Der Schoot, S. Jeanneret, A. Manz, H. M. Widmer and N. F. De Rooij, Three-dimensional micro flow manifolds for miniatured chemical analysis systems, *Journal of Micromechanics and Microengineering*, 4 (1994) 246-256.
[4] P. A. Auroux, D. Iossifidis, D. R. Reyes and A. Manz, Micro total analysis systems. 2. Analytical standard operations and applications, *Analytical Chemistry*, 74 (2002) 2637-2652.
[5] P. A. Auroux, D. Iossifidis, D. R. Reyes and A. Manz, Micro total analysis systems.1. Introduction, theory, and technology, *Analytical Chemistry*, 74 (2002) 2623-2636.
[6] V. Singhal and S. V. Garimella and A. Raman, *Microscale pumping technologies for microchannel cooling systems*, BIRCK and NCN publications, 57 (2004) 191-221.
[7] S. L. Zeng, C. H. Chen, J. C. Mikkelsen Jr. and J. G. Santiago, Fabrication and characterization of electroosmotic micropumps, *Sensors and Actuators B: Chemical*, 79 (2001) 107-114.
[8] V. L. Asuncion and P. L. Abraham, An AC magnetohydro dynamic micropump, *Sensors and Actuators B: Chemical*, 63 (2000) 178-185.
[9] F. Mugele and J. Baret, Electrowetting: from basics to applications, *Journal of Physics: Condensed Matter*, 17 (2005) 705-774.
[10] P. Gravesen, J. Braebjerg and O. S. Jensen, Microfluidics - a Review, *Journal of Micromechanics and Microengineering*, 3 (1993) 168-182.
[11] J. Dopper, M. Clemens, W. Ehrfeld, S. Jung, K. Kamper and H. Lehr, Micro gear pumps for dosing of viscous fluids, *Journal of Micromechanics and Microengineering*, 7 (1997) 230-232.
[12] A. Hatch, A. E. Kamholz, G. Holman, P. Yager and K. F. Bohringer, A ferrofluidic magnetic micropump, *Journal of Microelectromechanical System*, 10 (2001) 215-221.
[13] R. Wiederkehr, M. Salvadori, J. Brugger, F. Degasperi and M. Cattani, The gas flow rate increase obtained by an oscillating piezoelectric actuator on a micronozzle, *Sensors and Actuators A: Physical*, 144 (2008) 154-160.
[14] J. Dopper, M. Clemens, W. Ehrfeld, S. Jung, K. Kamper and H. Lehr, Micro gear pumps for dosing of viscous fluids, *Journal of Micromechanics and Microengineering*, 7 (1997) 230-232.
[15] C. Yamahata, M. Chastellain, V. Parashar, A. Petri, H. Hofmann and M. Gijs, Plastic micropump with ferrofluidic actuation, *Journal of Microelectromechanical System*, 14 (2005) 94-102.
[16] A. Olsson, G. Stemme and E. Stemme, A valve-less planar fluid pump with two pump chambers, *Sensors and Actuators A: Physical*, 47 (1995) 549-556.
[17] A. Olsson, P. Enoksson, G. Stemme and E. Stemme, Micromachined flat-walled valveless diffuser pumps, *Journal of Microelectromechanical System*, 6 (1997) 161-166.
[18] E. Stemme and G. Stemme, A valveless diffuser /nozzle based fluid pump, *Sensors and Actuators A: Physical*, 39 (1993) 159-167.
[19] K. S. Yang, I. Y. Chen, K. H. Chien and C. C. Wang, A numerical study of the nozzle/diffuser micropump, *Journal of Mechanical Engineering Science*, 222 (2008) 525-533.
[20] G. Krishnan and K. Mohseni, Axisymmetric Synthetic Jets: An Experimental and Theoretical Examination, *Aiaa Journal*, 47 (10) (2009) 2273-2283.

[21] D. J. Tritton, *Physical Fluid Dynamics*, Van Nostrand Reinhold, Canada (1977).

[22] C. Y. Gan, K. S. M. Sahari and Ch. S. Tan, Numerical investigation on Coanda flow over a logarithmic surface, *Journal of Mechanical Science and Technology*, 29 (7) (2015) 2863-2869.

[23] X. B. Luo and Zh. X. Luo, Principle and simulation of a novel non-valve micropump, *China Mechanical Engineering*, 15 (2002) 1261-1263.

[24] J. P. Choi, K. S. Kim, Y. H. Seo and B. H. Kim, Design and fabrication of synthetic air-jet micropump, *International Journal of Precision Engineering And Manufacturing*, 12 (2) (2011) 355-360.

[25] S. Yang, SH. Q. Yuan and X. H. Hua, Valveless piezoelectric micropump base on Coanda Effect, *Transactions of the Chinese Society for Agricultural Machinery*, 45 (11) (2014) 343-348.

[26] X. T. Zhang, Y. Song and X. H. He, A Bidirectional Valveless Piezoelectric Micropump With Double Chambers Applying Synthetic Jet, *Proceeding of the ASME-JSME-KSME Joint Fluid Engineering Conference*, Seoul, Korea (2015).

[27] Y. Ch. Wang, J. Ch. Hsu, P. Ch. Kuo and Y. Ch. Lee, Loss Characteristics and flow rectification property of diffuser valves for micropump applications, *International Journal of Heat and Mass Transfer*, 52 (1-2) (2009) 328-336.

[28] P. Gravesen, J. Branebjerg and O. S. Jensen, Microfluidics - a review, *Journal of Micromechanics and Microengineering*, 3 (4) (1998) 168-182.

[29] S. Li, A numerical study of micro synthetic jet and its applications in thermal management, *Ph.D. Thesis*, Georgia Institute of Technology, Atlanta, Georgia, USA (2006).

[30] L. Guo, W. Yan, Y. Xu and Y. Chen, Valveless piezoelectric micropump of parallel double chambers, *International Journal of Precision Engineering and Manufacturing*, 13 (5) (2012) 771-776.

Xiuhua He received the B.S. degree in Hydraulic Machinery from Zhenjiang Institute of Agricultural Machinery in 1982, the M.S. degree in Fluid Machinery and Hydrodynamic Engineering from Jiangsu University of Science and Technology in 1991, and the Ph.D. degree in Fluid Machinery and Engineering from Jiangsu University in 2010. She is currently a Professor at School of Energy and Power Engineering, Jiangsu University, China. Her research interests include the performance and internal flow of fluid machinery.